HAMAMATSU PRESENTS

ANALYTICAL TALKS

WATCH NOW ▶

SPECIAL ISSUE - RESEARCH ARTICLE

Quantification of the nonlinear susceptibility of the hydrogen and deuterium stretch vibration for biomolecules in coherent Raman micro-spectroscopy

Dale Boorman[1] | Iestyn Pope[1] | Francesco Masia[1] | Peter Watson[1] | Paola Borri[1] | Wolfgang Langbein[2]

[1]School of Biosciences, Cardiff University, Cardiff, UK

[2]School of Physics and Astronomy, Cardiff University, Cardiff, UK

Correspondence
Wolfgang Langbein, Cardiff University, School of Physics and Astronomy, The Parade, Cardiff CF24 3AA, UK.
Email: langbeinww@cardiff.ac.uk

Abstract

Deuterium labelling is increasingly used in coherent Raman imaging of complex systems, such as biological cells and tissues, to improve chemical specificity. Nevertheless, quantitative coherent Raman susceptibility spectra for deuterated compounds have not been previously reported. Interestingly, it is expected theoretically that –D stretch vibrations have a Raman susceptibility lower than –H stretch vibrations, with the area of their imaginary part scaling with their wavenumber, which is shifted from around 2900 cm^{-1} for C–H into the silent region around 2100 cm^{-1} for C–D. Here, we report quantitative measurements of the nonlinear susceptibility of water, succinic acid, oleic acid, linoleic acid and deuterated isoforms. We show that the –D stretch vibration has indeed a lower area, consistent with the frequency reduction due to the doubling of atomic mass from hydrogen to deuterium. This finding elucidates an important trade-off between chemical specificity and signal strength in the adoption of deuterium labelling as an imaging strategy for coherent Raman microscopy.

KEYWORDS

CARS, coherent Raman, deuterium, isotopes, Raman

1 | INTRODUCTION

Raman micro-spectroscopy is increasingly used as a label-free, chemically specific imaging modality in cell biology.[1] Spontaneous Raman scattering cross-sections of biomolecules, however, are notoriously small, with corresponding limitations in imaging speed and sensitivity. The development of coherent Raman scattering (CRS) microscopy[2] is partially circumventing these limitations, owing to the constructive interference of

Raman scattering by identical bonds in the focal volume, coherently driven to vibrate in phase. Many of the earlier demonstrations of CRS microscopy[3,4] showed images acquired at a single vibrational resonance, often chosen at the CH_2 symmetric stretch vibration around 2850 cm^{-1} wavenumber, which is abundant in lipids. It was soon realized, however, that this approach offered limited chemical specificity, considering that many biomolecules have C–H bonds and that the C–H stretch region is congested with several overlapping resonances.

Substituting hydrogen with deuterium offers a simple way to increase chemical specificity, considering that C–D stretch vibrations are shifted into the so-called silent region of the vibrational spectrum, around 2100 cm^{-1}, so that they can be easily distinguished. Indeed, deuterated compounds have been used extensively to provide specific chemical contrast when examining lipid bilayers,[5,6] drug delivery,[7] protein synthesis,[8] metabolic dynamics,[9] glucose metabolism,[10] and neurodegenerative disorders.[11]

Triggered by these developments, a basic question arises, namely, how is the magnitude of the Raman scattering cross-section changing upon deuterium substitution, and in turn, how is the CRS susceptibility *amplitude* scaling. In other words, besides introducing a vibrational resonance frequency shift, what are the implications of deuterium labelling on the Raman and CRS signal strength? Surprisingly, despite the fundamental nature of the question, there have been only few reports on the comparison of absolute Raman scattering cross-sections of molecules as function of their deuteration, and only by means of spontaneous Raman scattering, while a quantitative comparison of the CRS susceptibility of deuterated versus nondeuterated compounds is still missing.

In this work, we have quantitatively measured the nonlinear susceptibility strength for a series of deuterated compounds and compared the results with theoretical expectations derived from spontaneous and coherent Raman polarizability models. Measurements were carried out with our home-built hyperspectral coherent anti-Stokes Raman scattering (CARS) microscope and an in-house developed unsupervised quantitative data-analysis algorithm, which allows us to retrieve Raman-like spectra and spatially resolved concentration maps of chemical components, in physically meaningful units, with no prior knowledge.[12-15] With this method, we can determine the CRS susceptibility $\bar{\chi}$ in absolute units, by referencing it to the one of standard microscopy glass[16] which has a known nonlinear susceptibility. We have used the method to measure $\bar{\chi}$ of deuterated and nondeuterated isoforms of selected biological compounds, namely, water, succinic acid, oleic acid and linoleic acid. Additionally, the relative spontaneous Raman scattering intensities were measured and analysed.

The paper is organized as follows. In Section 2, we introduce the effect of changing isotopes for the Raman response, as predicted by the bond polarizability model. In Section 3, we provide details of materials and methods, and in Section 4, we report the measured Raman and $\bar{\chi}$ spectra for the compounds studied.

2 | ISOTOPE EFFECTS IN RAMAN SUSCEPTIBILITIES

2.1 | Spontaneous Raman scattering

In the bond polarizability model, the differential Raman cross-section of a vibrational mode l is given by[17] (see supporting information, Section S1)

$$\frac{d\sigma_l}{d\Omega} = \frac{\mu_0^2}{1440\pi^2} \frac{(\omega_0 - \omega_l)^4}{1 - \exp(-\hbar\omega_l/k_B T)} S_l, \quad (1)$$

where μ_0 is the vacuum permeability, ω_0 is the incoming light angular frequency, ω_l is the angular frequency of the vibrational mode, k_B is the Boltzmann constant and T the temperature. S_l is the scattering coefficient with can be expressed for unpolarized detection in a direction orthogonal to the excitation polarization as

$$S_l = 45(\bar{\alpha}_l')^2 + 7(\bar{\gamma}_l')^2, \quad (2)$$

where $(\bar{\alpha}_l')^2$ and $(\bar{\gamma}_l')^2$ are the invariants[18] of the derivative of the molecular polarizability tensor with respect to the dimensionless normal coordinate q_l. Here, $45(\bar{\alpha}_l')^2$ provides the isotropic (or trace) part, which is co-polarized to the excitation polarization, and $7(\bar{\gamma}_l')^2$ is the anisotropic part, of which $4(\bar{\gamma}_l')^2$ is co-polarized and $3(\bar{\gamma}_l')^2$ is cross-polarized. q_l is related to the coordinates x_i of the atom i with mass m_i in the molecule by

$$x_i = \sum_l q_l D_{li} \sqrt{\frac{\hbar}{\omega_l m_i}} \quad (3)$$

with the orthonormal transformation matrix D_{ij} describing the eigenmodes. Changing the mass of an atom by replacing it with an isotope preserves the electronic binding and thus the force constants K_{ij} of the vibrational dynamics. This leads to an approximate sum rule[19]

$$\sum_l \frac{S_l}{\omega_l} = s \quad (4)$$

with a constant s independent of the isotopes. While the sum extends over all vibrations of the molecule, due to the much smaller mass of both hydrogen and deuterium compared with other atoms, their stretching vibrations are often not significantly mixing with others. Hence, one can expect that the sum rule holds for the –H and –D

stretch vibrations alone, predicting that the scattering coefficient scales proportional to the vibrational frequency. We note that equivalent sum rules hold also for the infrared polarizability of the vibrational modes.[19,20]

A similar conclusion can be reached considering an isolated stretch vibration and an infinite mass of the C atom. In this case, we can use $\omega_l^2 = K_{ll}/m_l$, so that $x_l = q_l\sqrt{\hbar\omega_l/K_{ll}}$, and it follows that

$$(\bar{\alpha}_l')^2 = \left(\frac{\partial\bar{\alpha}}{\partial q_l}\right)^2 = \left(\frac{\partial\bar{\alpha}}{\partial x_l}\right)^2 \frac{\hbar\omega_l}{K_{ll}}, \tag{5}$$

and equivalently for $(\bar{\gamma}_l')^2$. Because the derivative of the polarizabilities versus x_l is a property of the electronic binding and therefore independent of the isotope mass, we find that the scattering coefficient is proportional to ω_l.

There have been only few experimental reports on the comparison of absolute Raman scattering cross-sections of molecules as function of their deuteration, and none directly addressed the theoretical prediction of a scattering coefficient scaling proportionally to the vibrational frequency. Let us summarize the experimental finding of these works in relation to the sum rule given by Equation (4). In Martín and Montero,[17] ethane was measured in the gas phase and fitted with a bond-polarizability model, followed by ethene[21] and benzene.[22] The reported scattering cross-sections for C–H and C–D stretch vibrations are used here to evaluate the sum rule prediction. The sum of the reported scattering coefficients S_l of the C–H stretching vibrations S_H (2800–3150 cm^{-1}) and the C–D stretching vibrations S_D (2100–2400 cm^{-1}) are shown in Figure 1

versus the deuteration number. The scattering coefficients are well described by a proportionality with the number of C–H and C–D bonds, respectively, yielding values of (S_H, S_D) per bond in units of 10^{-81} C^{2}m^{4}V^{-2} given by $(12.8, 9.3)$ for ethane, $(8.8, 5.6)$ for ethene, and $(13.6, 7.1)$ for benzene. The corresponding ratio $\varrho = S_H/S_D$ is 1.34 for ethane, 1.58 for ethene and 1.9 for benzene. Absolute measurement errors are estimated to be around 10% in these works.[17,21,22] The largest systematic uncertainty of the ratio is present in benzene where no partially deuterated data were reported. Let us now compare ϱ with the vibrational wavenumber ratios. For ethane, the average C–H stretch vibrations of C$_2$H$_6$ are at 2942 cm^{-1}, and the average C–D stretch vibrations of C$_2$D$_6$ are 2152 cm^{-1}, having a wavenumber ratio of 1.37. This is consistent with the measured ϱ. For ethene, the averages are 3051 cm^{-1} for of C$_2$H$_4$ and 2277 cm^{-1} for C$_2$D$_4$, yielding a ratio of 1.34, which is lower than the measured ϱ of 1.58. For benzene, the averages are 3068 and 2291 cm^{-1}, yielding a ratio of 1.34, which is significantly lower than the measured ϱ of 1.9. Evaluating the sum rule Equation (4) over all vibrations reported in other studies,[17,21,22] we find that the constant s changes by a factor 1.09 from C$_2$H$_6$ to C$_2$D$_6$, 0.824 from C$_2$H$_4$ to C$_2$D$_4$, and 1.16 from C$_6$H$_6$ to C$_6$D$_6$. The deviation from 1 (i.e., a constant s independent of the isotopes) is close to the reported measurement error; hence, we can conclude that the scaling of the scattering coefficients with the vibrational frequency for deuteration is approximately valid for these examples. Notably, considering the reduced masses of the C–D bond $\mu = \text{Da}/(1/2 + 1/12)$, and the C–H bond $\mu = \text{Da}/(1 + 1/12)$ and the scaling of the frequency with the reduced mass as $1/\sqrt{\mu}$, we expect a frequency ratio of 1.363, very close to the
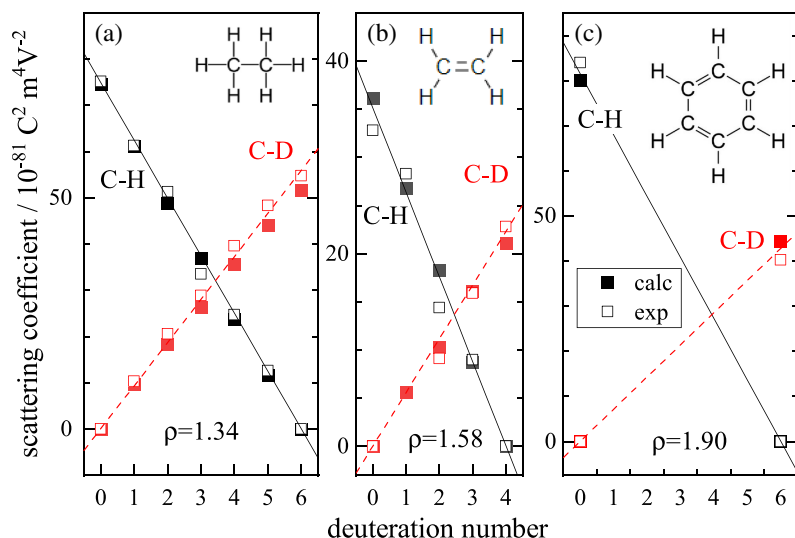
FIGURE 1 Raman scattering coefficients of the C–H stretch vibrations (around 3000 cm^{-1}) and corresponding C–D stretch vibrations (around 2200 cm^{-1}) for ethane[17] (a), ethene[21] (b) and benzene[22] (c), versus deuteration number. The open symbols are measured data; the closed symbols are results of a fit by a bond-polarizability model. Lines are fits proportional to bond number. The ratio ϱ between the scattering coefficient per bond for C–H relative to C–D corresponding to the fits is given

observed value for all molecules, confirming that the force constants K_{ll} are not significantly changed by deuteration.

For liquids, the effect of deuteration has been studied in water. Calibrated Raman scattering intensities are given in fig. 8 of Scherer et al.,[23] on the same scale for water (H_2O) and heavy water (D_2O), and are shown in Figure 2. The intensities were measured co-polarized ($I_{||}$) and cross-polarized ($I_\perp$) to the linear excitation polarization and are separated into the isotropic part $I_\alpha = I_{||} - I_\gamma$, shown as solid line, and the anisotropic part $I_\gamma = \frac{4}{3}I_\perp$, shown as dashed line. I_α corresponds to the scattering coefficient $S_l = 45(\bar{\alpha}_l')^2$ and I_γ to $4(\bar{\gamma}_l')^2$ in Equation (1). Integrating the Raman intensities over the bands shown in Figure 2 and scaling the integrated intensities with ($\omega_0 - \omega_l$)$^{-4}$ (the thermal occupation $\exp(-\hbar\omega_l/k_BT)$ is less than 10^{-4} at room temperature for wavenumbers above $2000\,\mathrm{cm}^{-1}$ and thus can be neglected for C–D and C–H stretch vibrations), where we have assigned a centre wavenumber of $3300\,\mathrm{cm}^{-1}$ for H_2O and $2450\,\mathrm{cm}^{-1}$ for D_2O, we find a ratio of $\varrho = 1.44$ for I_α and 1.42 for I_γ, while the wavenumber ratio is 1.35. This is in reasonable agreement with the expected scaling. Because the Raman spectra are rather broad, we have also evaluated the sum rule directly, using the integrals of the intensities scaled by $\omega^{-1}(\omega_0 - \omega)^{-4}$ (see thin lines in Figure 2), yielding the ratio of 1.07 for I_α and 1.06 for I_γ and thus showing a deviation from the sum rule below 10%.

The Raman cross-sections H_2O and D_2O in gaseous form are reported in Avila et al.[24] tab. 3, for an excitation wavelength of 514.5 nm at $T = 300$ K. Using the centre frequencies of the dominating Q branch of ν_1 at 3650

and $2670\,\mathrm{cm}^{-1}$, we find a ratio $\varrho = 1.44$ for $I_{||}$ and 1.45 for $I_\perp$, with a wavenumber ratio of 1.37, similar to liquid water.

2.2 | Coherent Raman scattering

CRS uses two incident light fields, called pump and Stokes, to coherently drive molecular vibrations at the frequency difference between these two fields. The coherent Raman susceptibility for a simple harmonic oscillator of frequency ω_l, mass m_l, is given by[25]

$$\chi_R = \frac{\epsilon_0 N}{6m_l}\left(\frac{\partial\alpha}{\partial x_l}\right)^2 (\omega_l^2 - \Delta^2 + 2i\Delta\gamma)^{-1}, \qquad (6)$$

where $\Delta = \omega_P - \omega_S$ is the difference between the pump and Stokes angular frequency, N is the density of oscillators and $\partial\alpha/\partial x_l$ is the derivative of the polarizability versus the position coordinate. Close to resonance, $|\Delta/\omega_l \pm 1| \ll 1$, we can approximate χ_R as (see supporting information, Section S2)

$$\chi_R \approx \frac{\epsilon_0 N}{12m_l\omega_l}\left(\frac{\partial\alpha}{\partial x_l}\right)^2 (\omega_l \mp \Delta \pm i\gamma)^{-1}, \qquad (7)$$

having an imaginary part of

$$\mathrm{Im}(\chi_R) \approx \frac{\epsilon_0 N}{12m_l\omega_l}\left(\frac{\partial\alpha}{\partial x_l}\right)^2 \frac{\mp\gamma}{(\omega_l \mp \Delta)^2 + \gamma^2}. \qquad (8)$$
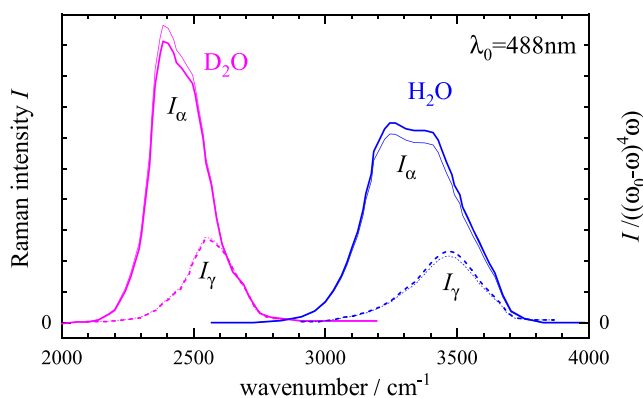
The area of $\Im(\chi_R)$ over the resonance is given by

$$A = \int \mathrm{Im}(\chi_R)d\Delta \approx \mp\frac{\pi\epsilon_0 N}{12m_l\omega_l}\left(\frac{\partial\alpha}{\partial x_l}\right)^2. \qquad (9)$$

Now, for isotope substitution, we can again use $\omega_l^2 = K_{ll}/m_l$, so that

$$A \approx \mp\frac{\pi\epsilon_0 N\omega_l}{12K_{ll}}\left(\frac{\partial\alpha}{\partial x_l}\right)^2. \qquad (10)$$

We therefore find that the area A is proportional to the vibrational angular frequency ω_l, hence follows the same scaling as the Raman scattering coefficient discussed in Section 2.1.

FIGURE 2 Raman scattering intensities[23] of water (H_2O, blue) and heavy water (D_2O, magenta) at 23°C using 488-nm excitation. The isotropic part I_α is shown as solid line, and the anisotropic part I_γ as dashed line. The intensities scaled by a factor $(\omega_0 - \omega)^{-4}\omega^{-1}$ are shown as thin lines

In terms of available experimental findings, a previous Raman and CARS study of deuterated compounds[26] compared the measured spontaneous Raman intensity of the C–D band to the intensity of the dimethyl sulfoxide (DMSO) solvent, and also showed a ratiometric CARS intensity analysis of a deuterated versus nondeuterated compound. The latter study however was carried out without retrieval of the CRS susceptibility, which for CARS intensities leads to a complicated response affected by the nonresonant background. We are not aware of a quantitative comparison of the CRS susceptibility of deuterated versus nondeuterated compounds.

3 | MATERIALS AND METHODS

3.1 | Materials

Pure (>99%) succinic acid (SA), a dicarboxylic acid and D4-succinic acid (D4-SA), with four deuterium atoms bound to carbons 2 and 3, were purchased from Sigma Aldrich (UK). Pure (>99%) oleic acid (OA—a monosaturated 18 C molecule with a *cis* double bond at the ninth carbon), D17-oleic acid (D17-OA—having 17 deuterium atoms attached to carbons 11–18), linoleic acid (LA—a biunsaturated 18 C molecule with two *cis* double bonds at the ninth and twelfth carbons) and D11-linoleic acid (D11-LA—having 11 deuterium atoms attached to carbons 14–18) were purchased from Cayman Chemical (MI, USA). Heavy water (deuterium oxide, 99.9% deuterated) was purchased from Sigma Aldrich (UK),

and distilled water was purchased from Fisher Scientific (UK)—the structures of each of the investigated molecules are provided in Table S1.

3.2 | Sample preparation

Crystals of pure SA and D4-SA were formed by preparing a saturated solution of the compound dissolved in water at a temperature of 90°C and continuous mixing. After cooling to room temperature, 30 μl of the supersaturated solution was transferred into a well of 9-mm diameter, and 120-μm thickness formed using an adhesive imaging gasket (Grace BioLabs, OR, USA) attached on a 1-mm thick, 76 ×26 mm glass microscope slide (Thermo Scientific Menzel Gläser, UK). Samples were stored under humidified conditions to permit slow evaporation over 5 days, allowing large (about 500 μm sized) crystals to form (see inset in Figure 3). Crystals were enclosed with a glass coverslip (thickness #1.5, 25-mm diameter, PA, VWR International, USA) prior to imaging. OA, D17-OA, LA and D11-LA samples were prepared by transferring 10 μm of lipid solution (as provided by manufacturer; OA and LA in ethanol at 100 mg/ml, D17-OA and D11-LA in methyl acetate at 100 mg/ml) into the well formed by an imaging gasket attached on a microscope slide, and then evaporating the solvent under gentle nitrogen stream to leave only pure lipid. Consecutive 10 μl aliquots of solution were added and the solvent evaporated until a sufficiently large droplet of pure lipid was generated. The droplets were enclosed with a glass coverslip prior to
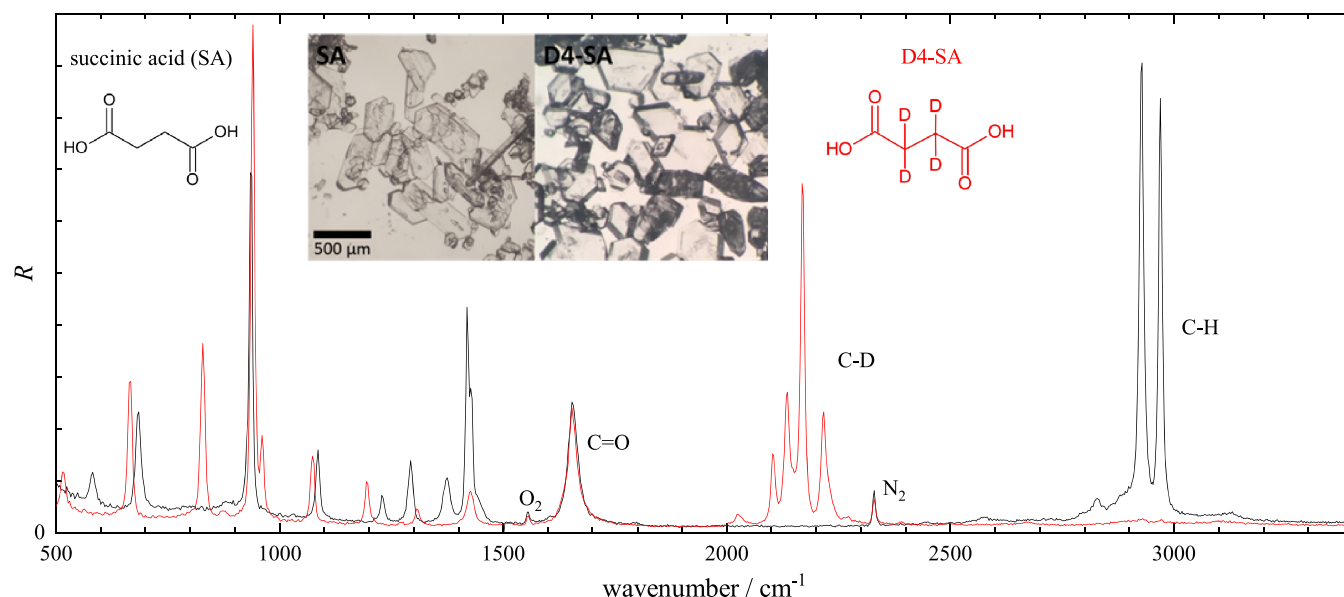
FIGURE 3 Scaled Raman scattering intensity R from pure SA and D4-SA crystals. Spectra are normalized to the area of their C=O peak at 1660 cm^{-1}. The peak area over the C–H range (2700–3200 cm^{-1}) is 4.35 for SA, and 0.14 for SA-D4 due to the O–H vibrations, while over the C–D range (1950–2450 cm^{-1}) the peak area is 3.39 for SA-D4 (not including the N$_2$ peak area). The inset shows representative transmission images of the investigated SA and D4-SA crystals

imaging. Water and heavy water samples were formed by transferring 13 μl of liquid into the centre of an imaging gasket on a glass microscope slide.

3.3 | CARS

CARS data were acquired using a custom-built multimodal laser scanning CARS microscope, the layout of which has been described in detail in our previous works.[15,27,28] In short, a Ti:Sa broadband (660 to 970 nm) pulsed laser (Venteon, Pulse:One PE) was pumped by a Nd:vanadate laser (Laser Quantum, Finesse) at 4.5 W to generate <8 fs pulses at a repetition rate of 80 MHz and with an average output power of 500 mW. A dichroic beamsplitter (CVI Melles Griot, LWP-450RP670-TP830-PW-1025-C) was used to separate (and then recombine) the laser beam into the pump and Stokes components, centred at 682 and 806 nm with a bandwidth (at 10% of the maximum) of 65 and 200 nm, respectively. Spectral focusing through linear chirping of pump and Stokes beams by glass blocks produced pulses of 1.5- and 5-ps duration, respectively, achieving a vibrational spectral resolution of 10 cm^{-1}. CARS spectra could be acquired over the range 1200–3800 cm^{-1} without adjustments to the laser, by automated control of the relative delay time between pump and Stokes pulses, and automated switching of detection filters and Stokes glass block thickness. Following recombination, the excitation beams were coupled into a commercial microscope stand (Nikon Ti-U) via a custom-built scanning head. Different objective and condenser combinations were used: a 60× 1.27NA water immersion objective (Nikon CFI Plan Apochromat IR λS, MRD70650) with a 1.34NA oil condenser (Nikon T-C-HNAO, MEL41410), as well as a 40× 1.15NA water immersion objective (Nikon CFI Plan Apochromat λS, MRD77410) or a 20× 0.75NA dry objective (Nikon CFI Plan Apochromat λ, MRD00205) with a 0.72NA dry condenser (Nikon T-C-CLWD, MEL56100). CARS signal from samples on microscope slides was collected in the forward direction by a photomultiplier tube (PMT) (Hamamatsu H7422-40). Use of double Semrock FF01-609/57, FF01-593/40 or FF01-562/40 bandpass filters permitted CARS imaging within the fingerprint (1200–1800 cm^{-1}), silent (1800–2600 cm^{-1}) and CH-stretch (2600–3700 cm^{-1}) regions of the Raman spectrum, respectively. Nonresonant CARS spectra were acquired from the glass coverslip under the same excitation and detection conditions and used for normalization to correct for the varying temporal overlap of pump and Stokes and to derive a CARS intensity ratio independent of excitation/detection parameters. Both xy sample motion and objective motion in z direction were motorized (Prior, ProScan III controller (V31XYZ), xy stage (H117NN2N) and z drive (PS3H122)).

Hyperspectral CARS was acquired using a pixel dwell time of 1 ms, and a PMT gain of 10^5. Typical excitation powers at the sample were 29 mW for the pump and 21 mW for the Stokes beam. Line scans of a few 10 μm width, having a few hundred pixels, were acquired over the nominal range 1600–4400 cm^{-1}, with 5-cm^{-1} step size. This range includes regions without temporal overlap, which were used for background subtraction.

The reference spectra in glass were taken using the same settings, moving the focus 40 μm into the coverslip glass.

A detailed description of the CARS data processing can be found in our previous works.[12,16,29] CARS intensity ratios were calculated by dividing background-corrected CARS intensities obtained from the investigated bulk materials (crystals or liquids) by the corresponding nonresonant CARS intensity measured in glass under the same excitation and detection conditions. The phase-corrected Kramers–Kronig method (PCKK) was then used to retrieve from the CARS intensity ratio spectra, $|\bar{\chi}|^2$, the complex CARS third-order susceptibility spectra, $\bar{\chi}$, normalized to the nonlinear susceptibility[30] $\chi^{(3)}_{1111} = n_0 n_2/(12\pi)$ of the glass used, with refractive index n_0 and nonlinear refractive index n_2. Considering the Schott D263 glass used for the coverslips in our study, we calculate $n_2 = 1.38 \times 10^{-13}$ esu using eq. 39 in Boling[31] with $\nu_d = 54.5$ and $n_d = 1.5231$. The units of $\bar{\chi}$ presented in this paper are accordingly 5.6×10^{-15} esu. The spectral calibration of the spectral focusing, providing the wavenumber calibration in the CARS data, has systematic errors similar to its spectral resolution.

3.4 | Spontaneous Raman scattering

Spontaneous Raman scattering was acquired using the same microscope as used for CARS described above. A 40× 0.95NA dry objective (Nikon CFI Plan Apochromat λS Series, MRD00405) was used for excitation and collection. The excitation beam from a 532-nm laser (Laser Quantum GEM) was passed through an exciter filter (Semrock LL01-532) and coupled into the microscope stand left port via a dichroic mirror (Semrock LPD01-532RS). Raman scattering was collected in epi-direction, transmitted through the dichroic and a long pass filter (Semrock BLP01-532R), dispersed by a spectrometer (Horiba Jobin-Yvon iHR 550) with a grating of 300 lines per millimetre blazed at 600 nm, and detected by a charge-coupled device (CCD) camera (Andor Newton DU971N-BV cooled to −60°C). Imaging of the intermediate image plane at the left port of the Ti-U

microscope stand onto a horizontal slit (Thorlabs VA100) and then onto the vertical input slit of the spectrometer provided confocality. The spectral resolution was $13\,\text{cm}^{-1}$. All measurements were performed with the samples at room temperature. The data were corrected by the spectral sensitivity, from sample to detection, calibrated using a radiometric calibration source (Ocean Optics LS-1-cal-int-22) to provide the intensity $I^R(\omega)$ proportional to the power per frequency across the spectrum. An exposure time of 20 s and an excitation power of about 100 mW at the sample was used.

4 | RESULTS

4.1 | Spontaneous Raman scattering

Spontaneous Raman spectral intensities I^R were acquired from the samples as described in Section 3.4. Spectra show a slowly varying background, likely due to fluorescence. This was accounted for in the following analysis using a baseline subtraction for the evaluation of areal integrals around relevant bands. Spectra were converted into the quantity $R = CI^R(\omega_0 - \omega)^{-4}\omega^{-1}$, to be able to directly evaluate the sum rule (4) by spectral integration. The normalization C was chosen to have a unity integral of R over the C=C and C=O peak at $1660\,\text{cm}^{-1}$, evaluated across the range 1600–$1750\,\text{cm}^{-1}$ using a linear baseline matching the end points. The resulting spectra for both nondeuterated and deuterated isoforms are shown in Figure 3 for succinic acid, Figure 4 for oleic

acid and Figure 5 for linoleic acid. The spectra clearly show the C–H and C–D stretch vibrations and a fingerprint region with more complex differences between deuterated and nondeuterated materials. The C–D and C–H peak areas in R were evaluated in the 1900–$2450\,\text{cm}^{-1}$ and 2600–$3200\,\text{cm}^{-1}$ range, respectively, using a linear baseline matching the end points. The results are given in Table 1, including the peak area per relevant bond. To evaluate the sum rule, the ratio η of the area per bond of C–H to C–D is also reported. We see that the determined η is in the 1.05 to 1.28 range, confirming the approximate validity of the sum rule for these substances, with deviations in the 10% to 20% range. This is similar to the result from previous reports on other substances given in Section 2.

Succinic acid (Figure 3) shows the sharpest vibrational lines, many of them resolution limited ($13\,\text{cm}^{-1}$), consistent with it being in crystalline form. The line arrangement shows that the crystal is in its more stable β form.[32] The vibrations in the C–H stretch range are the symmetric ($2924\,\text{cm}^{-1}$) and asymmetric ($2967\,\text{cm}^{-1}$) stretch.[32,33] We are not aware of a detailed line assignment for D4-SA. It is also interesting to note that because the area per C–H bond is close to unity relative to the C=O area (see Table 1), and considering that in a SA there are two C=O bonds, we can deduce that a C=O bond has about half the area of a C–H bond.

Oleic acid (Figure 4) shows generally broader vibrational lines because it is in liquid form. The C–H stretch region[34] shows a sharp $2850\,\text{cm}^{-1}$ peak due to the CH_2 symmetric stretch. The $2720\,\text{cm}^{-1}$ band is due a Fermi
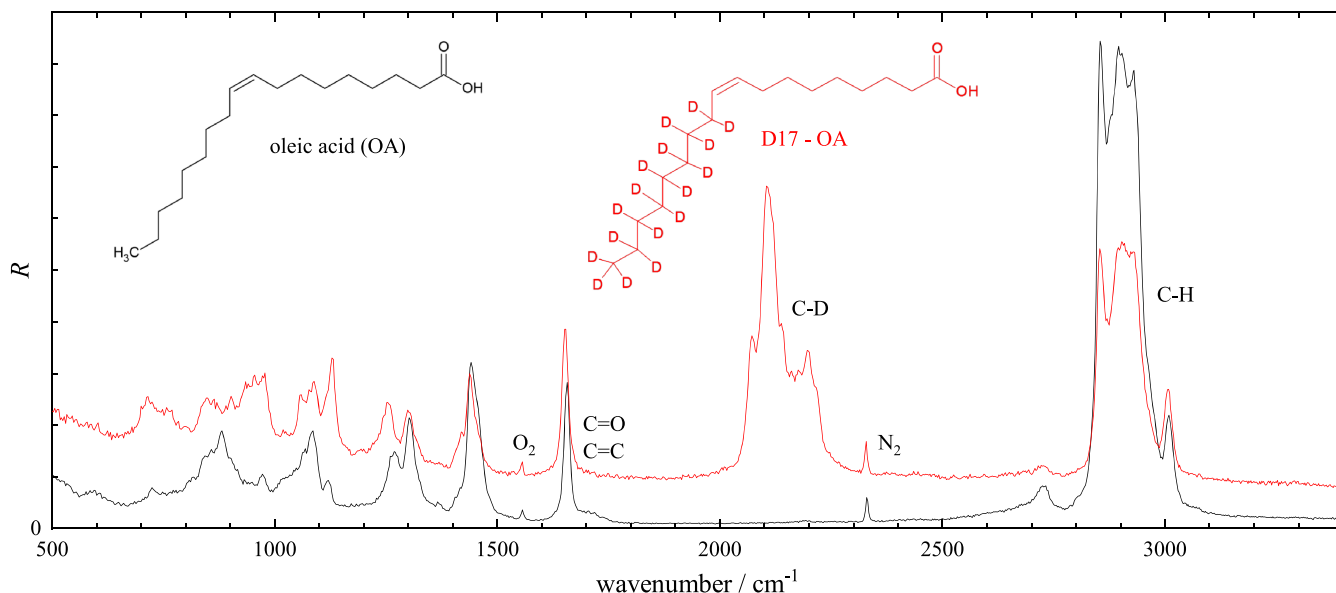
FIGURE 4 Scaled Raman scattering intensity R from oleic acid (OA) and D17-OA. Spectra are normalized to the area of the (C=O, C=C) peak at $1660\,\text{cm}^{-1}$ over the range 1600–$1750\,\text{cm}^{-1}$. The peak area over the C–H range (2600–$3200\,\text{cm}^{-1}$) is 18.5 for OA and 9.37 for D17-OA, while over the C–D range (1950–$2450\,\text{cm}^{-1}$), the peak area is 9.08 for D17-OA (not including the N_2 peak area)
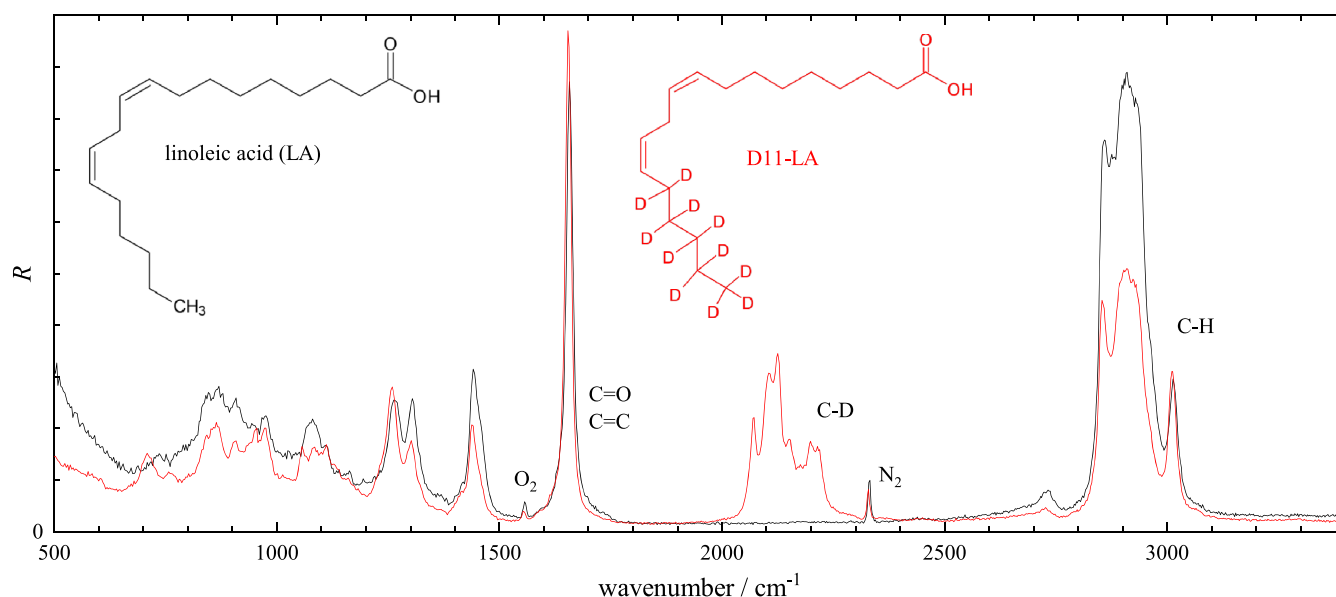
FIGURE 5 Scaled Raman scattering intensity R from linoleic acid (LA) and D11-LA. Spectra are normalized to the area of the (C=O, C=C) peak at 1660 cm^{-1} over the range 1600–1750 cm^{-1}. The peak area over the C–H range (2600–3200 cm^{-1}) is 5.27 for LA and 3.13 for D11-LA, while over the C–D range (1950–2450 cm^{-1}), the peak area is 1.56 for D11-LA (not including the N$_2$ peak area)

TABLE 1 Areas of the quantity R, for spontaneous Raman scattering, corresponding to the C–H and C–D stretch associated peaks, in units of the (C=O, C=C) peak area

Molecule	Bond	N_b	Area	Area/N_b	η
Succinic acid	C–H	4	4.35	1.09	1.28
D4-succinic acid	C–D	4	3.39	0.85	
Oleic acid	C–H	33	18.5	0.561	1.05
D17-oleic acid	C–H	16	9.37	0.586	1.10
	C–D	17	9.08	0.534	
Linolenic acid	C–H	31	5.27	0.170	1.20
D11-linolenic acid	C–H	20	3.13	0.157	1.11
	C–D	11	1.56	0.142	

Note: N_b is the number of bonds per molecules. The area per bond and the ratio η of the area per C–H bond to the area per C–D bond are also given.

resonance with the overtones of other CH$_2$ vibrations. The =C–H stretch gives rise to a band around 3010 cm^{-1}. The line at 1660 cm^{-1} used for normalization contains both the C=O and C=C stretch vibrations. Considering the area per C–H bond (Table 1) and assuming that the absolute scattering coefficients of the C–H bond and C=O bond are equal to those in SA, one can deduce that the C=C stretch has $2 \times 1.09/0.561 - 1 = 2.89$ times the area of the C=O stretch.

Linoleic acid (Figure 5) is also in liquid form. Compared with OA, the C–H stretch region shows a stronger =C–H stretch at 3010 cm^{-1} due to the presence of four of these bonds, instead of two in OA. The C=C stretch at

1660 cm^{-1} is enhanced even more, with a ratio to the =C–H stretch approximately double than that seen in OA. This indicates a coherent coupling between the two C=C bonds in LA, resulting in a single Raman active mode with twice the polarizability and thus four times the intensity. Considering the area per C–H bond (Table 1) and assuming again the same absolute area of the C–H bond and C=O bond as in SA, one can deduce that the double C=C stretch in LA has $2 \times 1.09/0.170 - 1 = 11.8$ times the area of the C=O stretch, which is very close to the value of $4 \times 2.89 = 11.6$ resulting from the coherent coupling model. Such coupling, both vibrational and electronic, is the mechanism allowing for large Raman cross-sections in polyynes,[35] which can be used as cellular labels.[36]

4.2 | CARS third-order susceptibility

The CARS spectra were acquired on the samples as described in Section 3.3. The measured CARS ratio $|\bar{\chi}|^2$ and the retrieved complex CARS susceptibility $\bar{\chi}$, in its real and imaginary part, are shown for both non-deuterated and deuterated isoforms, in Figure 6 for water, Figure 7 for succinic acid, Figure 8 for oleic acid and Figure 9 for linoleic acid.

We see that $|\bar{\chi}|^2$ covers two to three orders of magnitude across the spectral range, with a minimum above strong vibrational resonances due to the destructive interference between the positive nonresonant electronic response and the negative vibrationally resonant
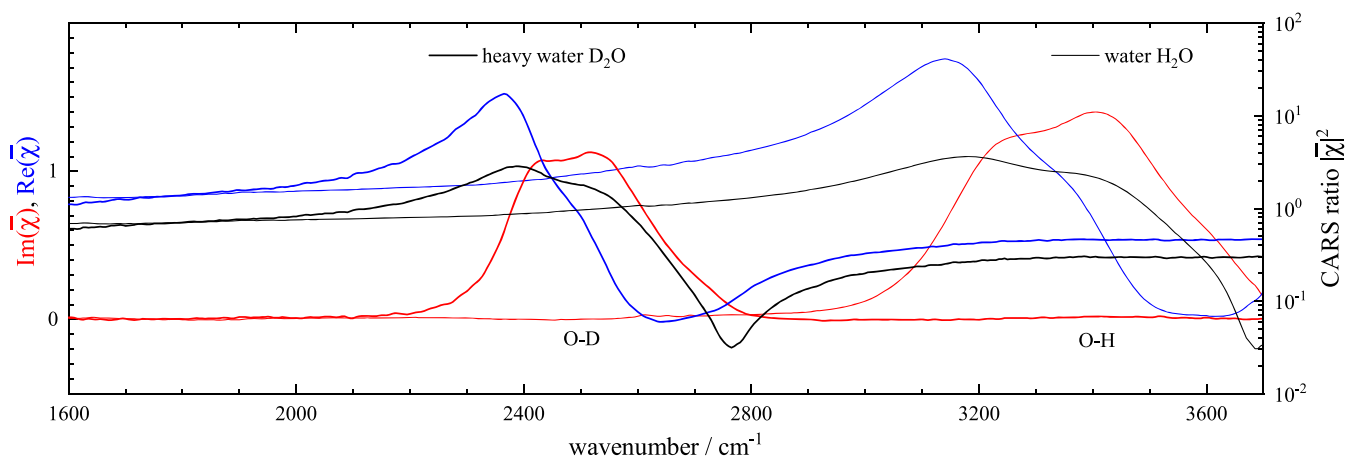
FIGURE 6 Coherent anti-Stokes Raman scattering (CARS) ratio $|\bar{\chi}|^2$ (black), and retrieved real (blue) and imaginary (red) part of the normalized CARS susceptibility $\bar{\chi}$, of water H_2O (thin lines) and heavy water D_2O (thick lines), at 20°C
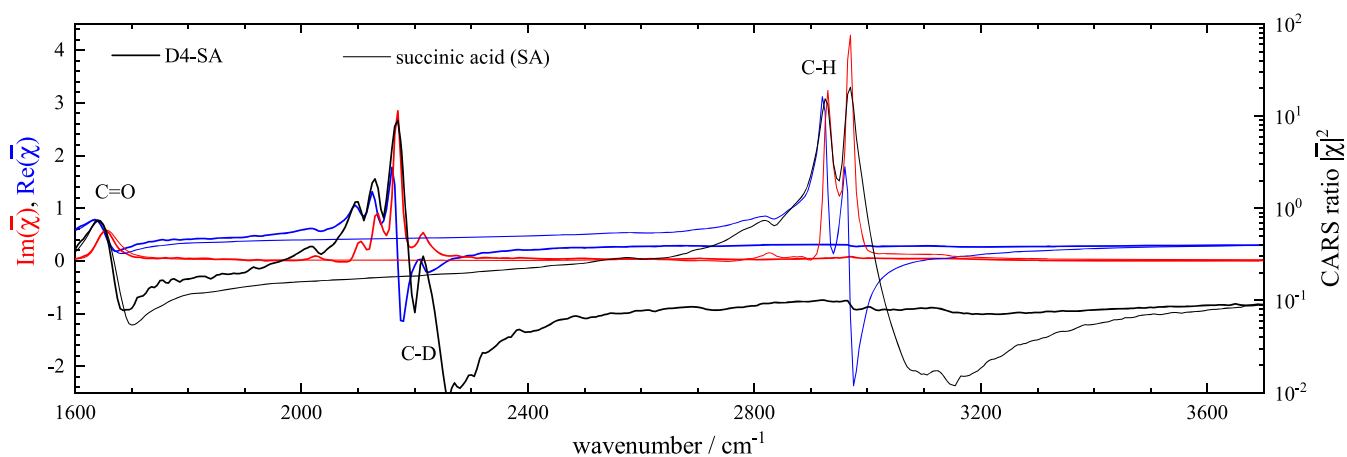
FIGURE 7 As Figure 6, for SA (thin lines) and D4-SA (thick lines)
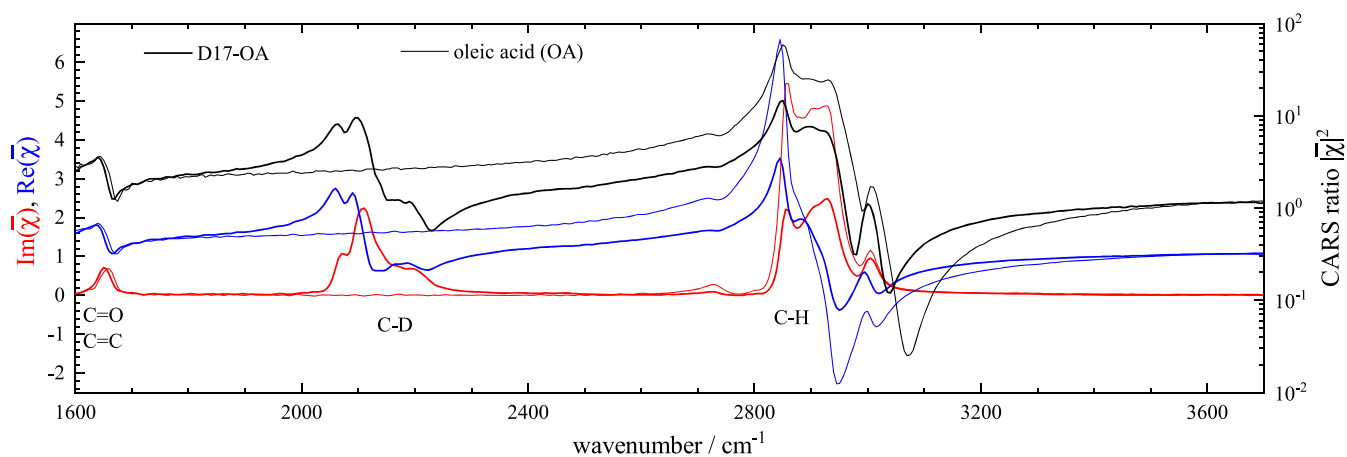
FIGURE 8 As Figure 6, for OA (thin lines) and D17-OA (thick lines)

response. This can be also clearly seen in the retrieved real part $\mathrm{Re}(\bar{\chi})$, which crosses zero in these spectral regions. Accurately measuring the CARS intensity over a dynamic range of 3 orders of magnitude can be challenging and requires suited acquisition parameters and background subtraction.

Generally, the $\mathrm{Im}(\bar{\chi})$ spectra resemble the Raman spectra shown in Figures 2–5 keeping in mind that the latter show R, which contains an additional ω^{-1} factor to directly represent the sum rule.

Starting with water and heavy water (Figure 6), we evaluate the O–H and O–D stretch peak areas in $\mathrm{Im}(\bar{\chi})$ over the ranges 2900–3700 cm^{-1} and 2100–2900 cm^{-1}, respectively, using a linear baseline matching the end points, with the results given in Table 2. Because $\mathrm{Im}(\bar{\chi})$ is scaling with the bond density in the focal volume, we evaluate the area per bond density A/N, using the bond density $N = DN_\mathrm{b}/M$, with the

molecular weight M, the mass density D and the number of bonds per molecule N_b. Note that the theoretical expression for A/N is given in Equation (10), showing a proportionality to the vibrational wavenumber under isotope substitution. The ratio ϱ of the area per bond density between –H and –D bonds is found to be 1.57, and using a vibrational wavenumber ratio of 1.35, the sum rule factor is $\eta = 1.16$, that is, the –H bonds have a 16% larger area than predicted by the sum rule.

Moving to succinic acid (Figure 7), the spectrally sharp resonances lead to a strong modulation of $\mathrm{Re}(\bar{\chi})$, reaching strongly negative values above resonance and a large maximum $\mathrm{Im}(\bar{\chi})$ of around 4. We evaluate C–H and C–D stretch peak areas in $\mathrm{Im}(\bar{\chi})$ over the ranges 2600–3250 cm^{-1} and 1950–2400 cm^{-1} using a linear baseline matching the end points. The results are again shown in Table 2, giving $\varrho = 1.70$ and a sum rule factor of $\eta = 1.26$.
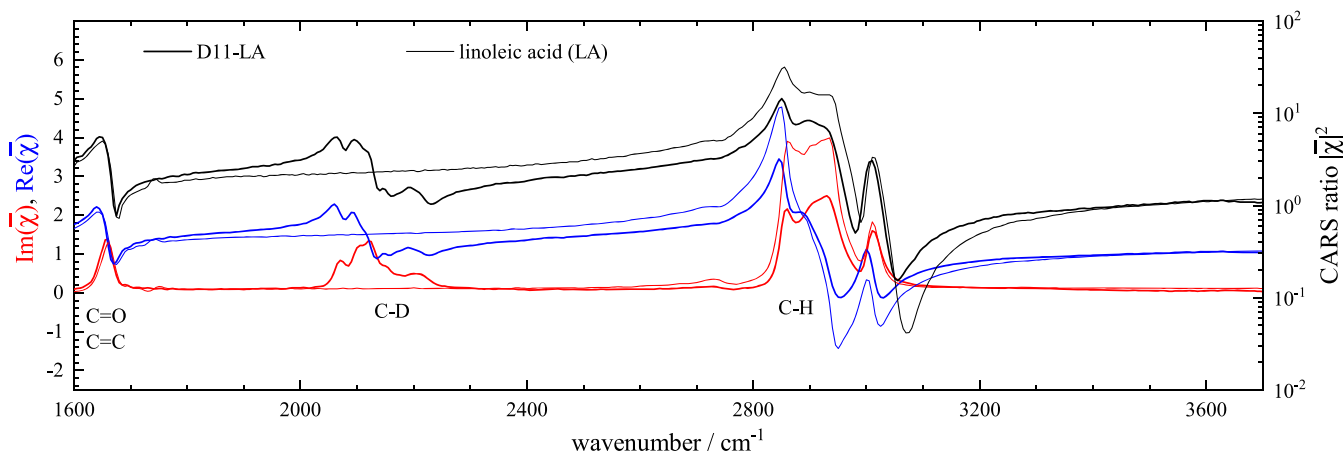

FIGURE 9 As Figure 6, for LA (thin lines) and D11-LA (thick lines)

TABLE 2 $\mathrm{Im}(\bar{\chi})$ peak areas (A) and derived quantities for O–H, O–D, C–H and C–D associated peaks across all investigated molecules

Molecule	Bond	N_b	A (cm^{-1})	N (nm^{-3})	A/N (cm^{-1} nm^3)	ϱ	η
H$_2$O	O–H	2	528	6.67	79.2	1.57	1.16
D$_2$O	O–D	2	336	6.67	50.4		
SA	C–H	4	167	3.18	52.5	1.70	1.26
D4-SA	C–D	4	98	3.18	30.8		
OA	C–H	33	619	6.29	98.4	1.63	1.20
D17-OA	C–H	16	300	3.05	98.4	1.63	1.20
	C–D	17	196	3.24	60.5		
LA	C–H	31	512	5.99	85.5	1.47	1.09
D11-LA	C–H	20	321	3.86	83.2	1.43	1.06
	C–D	11	123	2.12	58.0		

Note: N is the bond density, A/N is the area per bond density and ϱ is the ratio of A/N between –H and –D bonds. η is ϱ divided by the wavenumber ratio, which is predicted to be unity by Equation (10).

OA and LA fatty acids are shown in Figures 8 and 9. The large number of C–H stretch vibrations in OA leads to a large resonant response, with values of $\mathrm{Re}(\bar{\chi})$ spanning from -2 to $+6$, and $\mathrm{Im}(\bar{\chi})$ reaching 5. The peak areas are evaluated as above and are given in Table 2, resulting in $\varrho = 1.63$, both comparing the C–H in OA with the C–D in D17-OA, and for the C–H in D17-OA, corresponding to a sum rule factor of $\eta = 1.20$. Notably, the area per bond density A/N is nearly twice that in SA, indicating some coherent coupling within the long C–H chains.

For LA, the results are similar to OA. Notably, the C=C peak is stronger, consistent with the observation in Raman. The peak areas are evaluated as above and are again given in Table 2, resulting in $\varrho = 1.47$ comparing the C–H in LA with the C–D in D11-LA, and $\varrho = 1.43$ for the C–H in D11-LA, corresponding to sum rule factors of $\eta = 1.09$ and 1.06. This better agreement with the sum rule is mostly due to the reduction of the area per bond density A/N for the C–H bonds compared with OA.

Overall, the sum rule factors are similar to the ones observed in spontaneous Raman, see Table 1. We note that the accuracy of the retrieved areas is estimated to be better than 10%, limited by slightly different focusing for the reference spectrum taken in the coverslip glass, and the PCKK retrieval. However, we can see that the ratio ϱ seen in the deuterated compounds alone (D17-OA and D11-LA) and the ones seen comparing with separate measurements (OA and LA) show a maximum difference of 3%, indicating that systematics are in the few percentage range. The up to 20% higher area of the O–H and C–H vibrations than expected from the sum rule could be related to anharmonicity and coherent coupling effects.

5 | CONCLUSIONS

In conclusion, we have shown that the Raman scattering coefficients and the coherent Raman susceptibility $\bar{\chi}$ of the –H stretch vibrations approximately scale with the vibrational frequency under isotopic substitution of hydrogen to deuterium. This is consistent with theoretical expectations of a sum rule for the Raman polarizability. We have reported quantitative $\bar{\chi}$ spectra for four relevant substances, water, succinic acid, oleic acid and linoleic acid, and their deuterated isoforms. Generally, –H stretch vibrations have a susceptibility higher by approximately 50% than –D stretch vibrations.

These results highlight that deuterium isotope substitution, albeit providing a simple way to increase chemical specificity in Raman and CRS methodologies by shifting vibrational resonances to the silent region, is accompanied by a signal reduction. Our finding will be relevant to the growing field of Raman and CRS imaging and sensing applications using deuterium isotope-labelling, for example, to accurately estimate detection limits and quantitatively interpret the data.

CONFLICT OF INTEREST
There are no conflicts to declare.

DATA AVAILABILITY STATEMENT
Information about the data created during this research, including how to access it, is available from Cardiff University data archive (http://doi.org/10.17035/d.2021.0132639812).

ORCID
Iestyn Pope https://orcid.org/0000-0002-4104-0389
Francesco Masia https://orcid.org/0000-0003-4958-410X
Peter Watson https://orcid.org/0000-0003-0250-7852
Paola Borri https://orcid.org/0000-0002-7873-3314
Wolfgang Langbein https://orcid.org/0000-0001-9786-1023

REFERENCES
[1] J.-X. Cheng, X. S. Xie, *Science* **2015**, *350*, aaa8870.
[2] C. Zhang, J.-X. Cheng, *APL Phot.* **2018**, *3*, 90901.
[3] C. L. Evans, X. S. Xie, *Annu. Rev. Anal. Chem.* **2008**, *1*, 883.
[4] A. Zumbusch, W. Langbein, P. Borri, Progress in Lipid Research, **2013**.
[5] E. O. Potma, X. S. Xie, *Chem. Phys. Chem.* **2005**, *6*, 77.
[6] L. Li, H. Wang, J.-X. Cheng, *Biophys. J.* **2005**, *89*, 3480.
[7] B. G. Saar, L. R. Contreras-Rojas, X. S. Xie, R. H. Guy, *Mol. Pharmaceutics* **2011**, *8*, 969.
[8] L. Wei, Y. Yu, Y. Shen, M. C. Wang, W. Min, *Proc. Natl. Acad. Sci. USA* **2013**, *110*, 11226.
[9] L. Shi, C. Zheng, Y. Shen, Z. Chen, E. S. Silveira, L. Zhang, M. Wei, C. Liu, C. de Sena-Tomas, K. Targoff, W. Min, *Nat. Commun.* **2995**, *2018*, 9.
[10] L. Zhang, L. Shi, Y. Shen, Y. Miao, M. Wei, N. Qian, Y. Liu, W. Min, *Nat. Biomed. Eng.* **2019**, *3*, 402.

[11] K. Miao, L. Wei, *ACS Central Sci.* **2020**, *6*, 478.

[12] F. Masia, A. Glen, P. Stephens, P. Borri, W. Langbein, *Anal. Chem.* **2013**, *85*, 10820.

[13] C. D. Napoli, I. Pope, F. Masia, P. Watson, W. Langbein, P. Borri, *Biomed. Opt. Express* **2014**, *5*, 1378.

[14] F. Masia, I. Pope, P. Watson, W. Langbein, P. Borri, *Anal. Chem.* **2018**, *90*, 3775.

[15] A. Karuna, F. Masia, M. Wiltshire, R. Errington, P. Borri, W. Langbein, *Anal. Chem.* **2019**, *91*, 2813.

[16] A. Karuna, F. Masia, P. Borri, W. Langbein, *J. Raman Spectrosc.* **2016**, *47*, 1167.

[17] S. Martín, J. Montero, *J. Chem. Phys.* **1984**, *80*, 4610.

[18] G. Placzek, *Die Rayleigh und Raman Streuung, Handbuch der Radiologie*, (Eds: E. Marx), Vol. VI, Akademische Verlagsgesellshaft, **1934**, pp. 209.

[19] B. Crawford, *J. Chem. Phys.* **1952**, *20*, 977.

[20] E. B. Wilson Jr., J. C. Decius, P. C. Cross, *Molecular Vibrations: The Theory of Infrared and Raman Vibrational Spectra*, McGraw-Hill **1955**.

[21] M. Orduna, A. del Olmo, C. Domingo, S. Montero, *J. Mol. Struct.* **1986**, *142*, 201.

[22] J. M. Fernández-Sánchez, S. Montero, *J. Chem. Phys.* **1989**, *90*, 2909.

[23] J. R. Scherer, M. K. Go, S. Kint, *J. Phys. Chem.* **1974**, *78*, 1304.

[24] G. Avila, J. Fernández, G. Tejeda, S. Montero, *J. Mol. Spectrosc.* **2004**, *228*, 38.

[25] R. W. Boyd, *Nonlinear Optics*, Elsevier **2008**.

[26] G. Bergner, C. R. Albert, M. Schiller, G. Bringmann, T. Schirmeister, B. Dietzek, S. Niebling, S. Schlcker, J. Popp, *Analyst* **2011**, *136*, 3686.

[27] I. Pope, W. Langbein, P. Watson, P. Borri, *Opt. Express* **2013**, *21*, 7096.

[28] I. Pope, F. Masia, K. Ewan, A. Jimenez-Pascual, T. C. Dale, F. A. Siebzehnrubl, P. Borri, W. Langbein, *Analyst* **2021**, *146*, 2277.

[29] F. Masia, A. Karuna, P. Borri, W. Langbein, *J. Raman Spectrosc.* **2015**, *46*, 727.

[30] R. Adair, L. L. Chase, S. A. Payne, *J. Opt. Soc. Am. B* **1987**, *4*, 875.

[31] N. Boling, A. Glass, A. Owyoung, *IEEE J. Quantum Electron.* **1978**, *14*, 601.

[32] A. R. Pallipurath, P.-B. Flandrin, L. E. Wayment, C. C. Wilson, K. Robertson, *Mol. Syst. Des. Eng.* **2020**, *5*, 294.

[33] V. Ananthanarayanan, *Proc. Indian Acad. Sci. A* **1960**, *51*, 328.

[34] C. Di Napoli, F. Masia, I. Pope, C. Otto, W. Langbein, P. Borri, *J. Biophotonics* **2014**, *7*, 68.

[35] N. R. Agarwal, A. Lucotti, M. Tommasini, W. A. Chalifoux, R. R. Tykwinski, *Phys, J. Chem. C* **2016**, *120*, 11131.

[36] F. Hu, C. Zeng, R. Long, Y. Miao, L. Wei, Q. Xu, W. Min, *Nat. Methods* **2018**, *15*, 194.

SUPPORTING INFORMATION

Additional supporting information may be found online in the Supporting Information section at the end of this article.